Structural characterization of lithium aluminosilicate glass and glass ceramics derived from spodumene mineral

1995 J. Phys.: Condens. Matter 7 3115

(http://iopscience.iop.org/0953-8984/7/16/007)

J. Phys.: Condens. Matter 7 (1995) 3115–3128. Printed in the UK

Structural characterization of lithium aluminosilicate glass and glass ceramics derived from spodumene mineral

A Nordmann†, Y-B Cheng†, T J Bastow‡ and A J Hill§

† Department of Materials Engineering, Monash University, Clayton, Victoria 3168, Australia
‡ CSIRO, Division of Materials Science and Technology, Private Bag 33, Rosebank MDC, Clayton, Victoria 3169, Australia
§ Faculty of Engineering, Monash University, Clayton, Victoria 3168, Australia

Received 7 November 1994, in final form 26 January 1995

Abstract. Lithium aluminosilicate (LAS) glass and glass ceramics derived from spodumene mineral have been studied by transmission electron microscopy (TEM), x-ray diffraction (XRD), positron annihilation lifetime spectroscopy (PALS) and solid state nuclear magnetic resonance (NMR) as as-cast glass, as partially crystallized glasses, and as fully crystalline glass ceramics. The nucleation and growth of the crystalline phases at 725 °C up to 1000 °C have been studied as functions of varying time and temperature. Both TEM and PALS are effective tools for studying the development of the nanophase structure in the partially crystallized glass. TEM observation established the size and number of crystallites present in the glassy matrix, whilst the PALS component attributed to orthopositronium (oPs) pickoff annihilation was remarkably sensitive to the nucleation and growth of the crystalline phases in the glass ceramic. This oPs component was associated either with the nuclei/glass interface or with the nuclei structure. XRD and NMR were used to study the evolution of the two crystalline phases which form from the glass in the temperature range 725 °C to 1000 °C, the β-quartz solid solution (SS) phase below 900 °C and the β-spodumene SS phase above 900 °C. The ^{29}Si NMR spectra of both β-quartz SS and β-spodumene SS phases show structures associated with the next nearest neighbour configurations of the central SiO_4 units. The ^{29}Si and ^{27}Al NMR spectra of α-spodumene mineral and β-spodumene SS phase formed by annealing α-spodumene are compared to the spectra for the glass and crystalline phases formed from the melt.

1. Introduction

The viability of producing glasses and glass ceramics in the Li_2O–Al_2O_3–SiO_2 (LAS) system has been recognized for many years and continues to attract attention from both the scientific and economic viewpoints. An understanding of the structure of both the parent glass and the crystallized product is crucial since it influences the mechanical, optical and especially the thermal properties of these materials.

The important crystalline phases obtained from the LAS system are β-quartz solid solution (SS) and β-spodumene SS, both of composition $Li_2O \cdot Al_2O_3 \cdot 4SiO_2$. Beta-quartz SS is a solid solution based on the hexagonal high-quartz structure and has a thermal expansion coefficient $\alpha_{20-700\ °C} = 0 \pm 0.15 \times 10^{-6}\ °C^{-1}$ [1]. Beta-spodumene SS is a solid solution derived from the tetragonal form of silica known as keatite and has a thermal expansion coefficient $\alpha_{20-700\ °C} = 1\text{–}2 \times 10^{-6}\ °C^{-1}$ [1]. It is generally reported that β-quartz SS transforms to β-spodumene SS at approximately 850–900 °C [1].

Conventionally, LAS glasses and glass ceramics are prepared by combining appropriate quantities of Li_2O (usually as Li_2CO_3), Al_2O_3 and SiO_2 in the required ratios and then

0953-8984/95/163115+14$19.50

melting the batch mixture at high temperatures to form a glass. If a glass ceramic is required, the component undergoes an appropriate heat treatment to produce the fully crystalline material. In the present work, however, the naturally occurring mineral, α-spodumene, has been used as the raw material. The α-spodumene mineral has a chain silicate structure whereas the two crystalline modifications (β-quartz SS and β-spodumene SS) have three-dimensional aluminosilicate frameworks in which the aluminium and silicon atoms are randomly distributed on the crystal lattice sites. The low thermal expansion coefficients of β-quartz SS and β-spodumene SS can be rationalized in terms of strong (Al, Si)–Li repulsive forces [2, 3]. The mineral α-spodumene has density $D_x = 3.177$ g cm^{-3} [4] whereas β-quartz SS and β-spodumene SS have density $D_x = 2.374$ g cm^{-3} [3].

With the aid of a nucleating agent (such as the TiO_2 used in the present work) the β-quartz SS phase can be prepared by heat treating the glass between 700 °C and 900 °C for 4 to 8 hours and the β-spodumene SS phase by heat treating above 900 °C. Details of this work, discussing the effect of nucleating agents, heat treatment time and heat treatment temperature on the nucleation and crystallization behaviour of the LAS system, will be published at a later date.

Solid state NMR has developed rapidly over the past 15 years as an atomic probe of materials, offering an attractive, element-specific, form of materials analysis [5, 6]. Of interest in the present work is the ability of NMR chemical shifts to distinguish between the glass and different crystalline structures, thereby providing quantitative analyses of phase content and bonding environment, both of which are unavailable from XRD [5]. The chemical shift mechanism relies on relatively close-range interactions so that a well defined resonance may be obtained in solids in the absence of long-range order.

Lithium aluminosilicates appear to offer three attractive nuclei with good abundance for structural investigation: ^{7}Li, ^{27}Al, and ^{29}Si (^{17}O generally requires enrichment). However ^{7}Li ($I = \frac{3}{2}$, $Z = 3$) has a chemical shift range too small to be useful as a probe. Of the remaining two nuclei, ^{29}Si offers the sharper probe of structure and atomic disorder. In the present work, ^{27}Al and ^{29}Si MAS NMR are used to probe the glass and crystalline structures of the $LiAlSi_2O_6$ system formed by various heat treatments.

Positron annihilation has been used for many years to characterize the electronic structure of condensed matter [7, 8]. Correlation of positron data with the chemical, electrical and physical properties of glasses has been successful in numerous systems including Li_2O–Al_2O_3–SiO_2 [9, 10]. The positron annihilation lifetime spectroscopy (PALS) technique involves using a positron source, such as ^{22}Na, to emit positrons into a sample. In inorganic glasses the PALS lifetime spectra typically can be modelled by two or three decaying exponentials, each with a particular lifetime τ_i (annihilation rate^{-1}) and intensity I_i (relative number of annihilations). The lifetime assignments in inorganic oxide glasses can be made as follows [10]:

τ_1 120–300 ps free positrons in the bulk and pPs self-annihilation,

τ_2 300–900 ps positron-oxygen bound states, positrons trapped at free volume sites (defects), and

τ_3 900–4000 ps oPs pickoff annihilation in free volume sites.

In crystalline ceramics the components in the lifetime spectra can be assigned as follows:

τ_1 120–400 ps free positrons annihilating in the bulk and possibly pPs self-annihilation,

τ_2 400–800 ps positrons trapped at defect sites (defects include anti-site, neutral vacancies, cation vacancies, vacancy clusters), and

τ_3 900–4000 ps oPs pickoff annihilation at interfacial spaces or surfaces.

In glasses and ceramics, the trapped positron component (τ_2, I_2) has been used to follow structural changes which affect the electron density at the trapping site such as the effect of dopant concentration in heavy-metal glasses [10] and the effect of irradiation and annealing on vacancy formation and clustering in SiC [11]. In glass ceramics the oPs pickoff component (τ_3, I_3) has been used to follow phase separation in lithium silicate glasses [12]. The goal of PALS research is identification of the annihilation mechanism and correlation of the annihilation parameters with properties of condensed matter. In addition, the non-destructive nature of PALS lends the technique to quality control applications, hence correlation of PALS parameter changes with microstructural changes due to processing is a burgeoning area of study.

The present work addresses the use of NMR and PALS in conjunction with traditional materials characterization techniques such as TEM and XRD to examine the nucleation and crystallization of LAS glass and glass ceramics as functions of heat treatment. Direct methods of bulk structure determination, such as XRD and TEM, are complemented by NMR and PALS observations of local bonding environments. Since the materials under consideration are derived from natural spodumene mineral, the natural and heat treated spodumene minerals have also been studied by these techniques.

2. Experimental details

2.1. Materials preparation

Glasses were prepared from a mixture containing 95 wt% spodumene concentrate (95% $LiAlSi_2O_6$, 5% SiO_2), 4 wt% TiO_2 as a nucleating agent and 1 wt% As_2O_3 as a fining agent to remove bubbles. The batch mixture was heated at 1600 °C for 3.5 h in a platinum crucible followed by water quenching. The glass was subsequently crushed and remelted under the same conditions twice more to ensure homogeneity. Following final melting, the glass was water quenched, transferred to an annealing oven and furnace cooled to room temperature. Glass samples approximately 1 cm × 1 cm × 2 mm thick were obtained by cutting larger glass fragments using a diamond saw. Heat treatment involved placing the glass samples on an alumina tray, heating to various temperatures (725 °C to 1000 °C), and holding for various times (1 h to 16 h). The heating and cooling rate was 5 °C min^{-1}. Both α- and β-spodumene minerals were studied by PALS and NMR and the results allowed for comparison of the data between the minerals and the crystallized glass ceramics. The α-form of spodumene was the natural mineral and the β-spodumene form was obtained by annealing the α-spodumene mineral at 1000 °C for 3 hours.

2.2. Materials characterization

XRD experiments were performed at room temperature (22 °C) using a Rigaku Geigerflex diffractometer and Ni-filtered Cu Kα radiation. Samples for TEM were ultrasonically cut, polished, ion beam milled to perforation, carbon coated and then examined in a Phillips EM420 TEM operating at 120 kV. Due to rapid degradation of the glassy samples by the electron beam in a conventional double-tilt holder, some samples were contained in a liquid-nitrogen-cooled holder.

The NMR data were obtained on powdered samples at ambient temperature (23 °C) with a Bruker MSL 400 spectrometer operating at a nominal field of 9.4 T, using two different double-bearing MAS probes. For ^{29}Si the specimens were spun in a 7 mm diameter PSZ rotor at approximately 4.3 kHz and single-pulse spectra were collected using a 5 μs pulse

and a repetition time of 20 s. For ^{27}Al spectra the samples were spun in a 4 mm PSZ rotor at approximately 10 kHz, and a pulse length of 0.7 μs and a repetition time of 1 s were used. Tetramethyl silane at 0 ppm was used as the reference for ^{29}Si; yttrium aluminium garnet ($Y_3Al_5O_{12}$), with an octahedral line at 0.7 ppm, was used as a reference material for ^{27}Al. The pulse repetition times of 20 s and 1 s used for accumulation of the ^{29}Si and ^{27}Al spectra respectively, were sufficient to prevent saturation.

The source for PALS experiments was made using aqueous $^{22}NaCl$, with an activity of about 20 μCi, which was evaporated onto a 2.5 μm thick annealed Ti foil (0.114 mg cm^{-2}) and covered by a second foil. The resulting foil sandwich was crimp sealed. The lifetime measurements were performed using a fast–fast coincidence spectrometer. The equipment was thermally stabilized at 22 ± 0.5 °C. The resolution function measured using ^{22}Na had a full width at half maximum (FWHM) value of 250 ps. The positron lifetime spectra contained about 1×10^6 counts. The spectra were evaluated using the program PFPOSFIT [13] to fit the data as the sum of decaying exponentials. The source component was detected using annealed aluminium standards which gave repeatable spectra of $\tau_1 = 166 \pm 1$ ps (intensity $I_1 = 98 \pm 0.5\%$) attributed to the Al and $\tau_2 = 450 \pm 35$ ps ($I_2 = 2 \pm 0.5\%$) attributed to the NaCl. Hence a source correction of $\tau_2 = 450$ ps, $I_2 = 2\%$ for annihilations taking place in the NaCl was used in the data analysis.

Samples were polished in order to minimize trapping of positrons at the surface, and two identical samples were placed on either side of the source sandwich. All spectra were collected at 22 ± 0.5 °C. Four to 10 spectra were collected for each sample, and the mean values with population standard deviations are reported. An additional error analysis based upon the least-squares fit of each spectrum is computed by the fitting program giving standard deviations on each lifetime component and a 'variance of the fit' defined by the ratio of the minimized sum of differences (between data and model) to the degrees of freedom [14]. This variance is normally distributed with a mean of unity. In the present work variances of the fit were less than 1.3 for the best fit whether a free or fixed fit. An attempt was made to fit all spectra with three free components (τ_1, I_1; τ_2, I_2; τ_3, I_3); however, not all spectra would converge with this degree of freedom. If convergence was not obtained in all spectra for a given sample, the short lifetime τ_1 was fixed at the mean value of τ_1 calculated from the spectra that did converge. This procedure allowed the fitting routine to converge for most spectra. The zero-time channel and the resolution function did not vary over the course of the experiments. Each spectrum took approximately four hours to collect.

3. Results and discussion

3.1. XRD and TEM

Table 1 summarizes the phase content of samples subjected to various heat treatment schedules. As indicated, the samples are comprised of either glass, β-quartz SS or β-spodumene SS. A typical XRD spectrum in which peaks were identified as β-quartz SS is presented in figure 1(a), while a typical β-spodumene SS spectrum is shown in figure 1(b).

Of particular interest in the present study is the crystallization behaviour occurring at 725 °C. As may be seen from table 1, a one-hour heat treatment at 725 °C maintained the fully amorphous nature of the as-cast glass. Increasing the time to 1.5 hours produced a sample in which both β-quartz SS and a glassy phase were detected. Further increments in heat treatment time at 725 °C generated samples which yielded diffraction peaks attributable only to β-quartz SS.

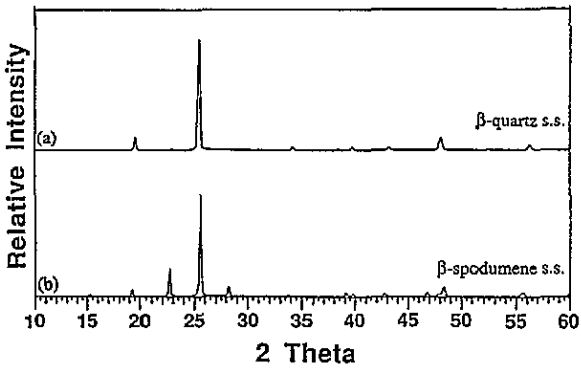

Figure 1. Representative XRD spectra of (a) β-quartz SS obtained by heat treatment of LAS glass at 750 °C for 4 h, and (b) β-spodumene SS, obtained by heat treatment of LAS glass at 950 °C for 4 h.

Table 1. Phase content of heat-treated samples.

Sample	Phase content
As-cast glass	Amorphous
1 h at 725 °C	Amorphous
1.5 h at 725 °C	Amorphous, β-quartz SS
4 h at 725 °C	β-quartz SS
6 h at 725 °C	β-quartz SS
8 h at 725 °C	β-quartz SS
16 h at 725 °C	β-quartz SS
4 h at 750 °C	β-quartz SS
4 h at 850 °C	β-quartz SS
4 h at 950 °C	β-spodumene SS
4 h at 1000 °C	β-spodumene SS

The actual XRD spectra for glasses heat treated at 725 °C for various times are presented in figure 2(a)–(c). The sample heated for 1 hour (figure 2(a)) shows the broad low-angle peak characteristic of an amorphous structure. A crystallization dwell time of 1.5 hours generates sharp diffraction peaks (indicating long-range order) consistent with crystalline β-quartz SS but superimposed on an amorphous background (figure 2(b)), and increasing the dwell time to 8 hours produces an XRD trace indicating total conversion to crystalline β-quartz SS.

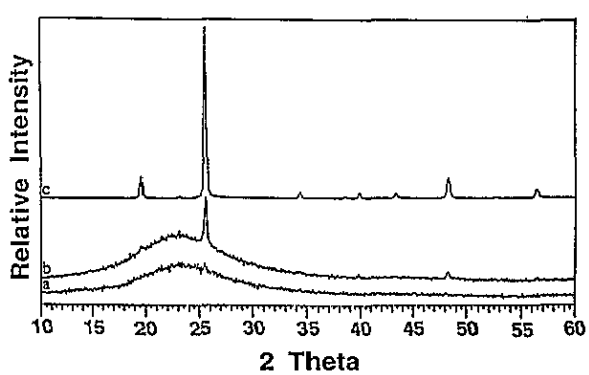

Figure 2. XRD spectra recorded from heat treated LAS glasses: (a) 1 h at 725 °C (amorphous), (b) 1.5 h at 725 °C (amorphous + β-quartz SS) and (c) 8 h at 725 °C (β-quartz SS).

TEM micrographs of the as-cast glass, as well as selected samples which have been heat

treated at 725 °C, are presented in figure 3(a)–(d). Figure 3(a) depicts a micrograph of the as-cast glass which reveals a homogeneous, inclusion-free structure. Heat-treating this glass for 1.5 hours at 725 °C (figure 3(b)) resulted in the formation of isolated nuclei, or nanocrystals (~ 50 nm diameter) of β-quartz SS, dispersed in the glassy matrix. Increasing the heat treatment time to 2 hours allowed these crystals to grow to an average diameter of approximately 100 nm (figure 3(c)), while an additional increment to 4 h led to further growth of these crystals so that their average diameter was about 120 nm (figure 3(d)). In all cases, XRD confirmed that the crystals were comprised of β-quartz SS. The XRD and TEM results indicate that the various stages of crystallization of the LAS glass may be controlled through judicious adjustments of the heat treatment time at 725 °C.

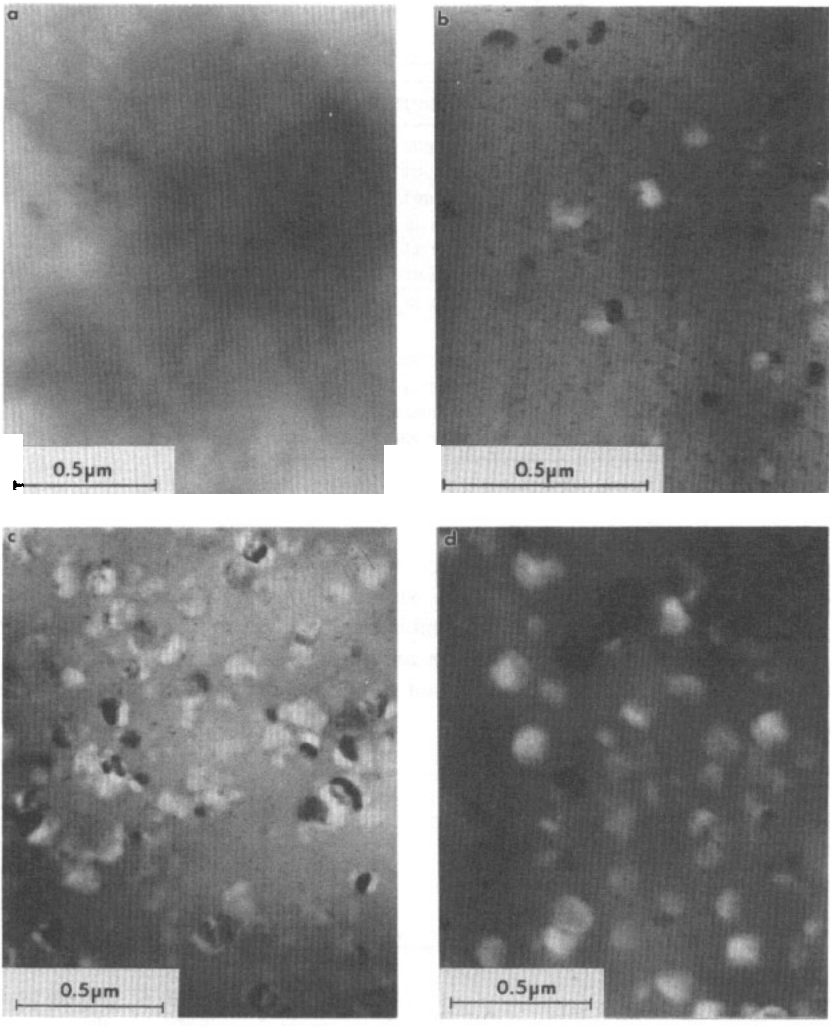

Figure 3. TEM micrographs of (a) as-cast LAS glass and LAS glasses heat treated at 725 °C for (b) 1.5 h, (c) 2 h and (d) 4 h.

In contrast, heat treatment at higher temperatures does not allow as much control over the crystallization behaviour. A fully crystalline microstructure always developed when

the heat treatment temperature was above 750 °C, regardless of the heat treatment time. For example, as indicated in table 1, crystallization at 750 °C and 850 °C for four hours generated samples comprised of β-quartz SS, whereas heat treatment at 950 °C and 1000 °C for 4 hours produced fully crystalline β-spodumene SS.

3.2. *NMR*

Figure 4 (a)–(f) presents the ^{29}Si NMR spectra for selected samples obtained during various stages of the crystallization process. Although the powder XRD indicates the presence of long-range lattice order after, say, 4 hours at 850 °C, the ^{29}Si NMR spectra reveal the presence of an additional disorder, viz. the interchange of Al and Si atoms bonded to the O atoms of the SiO_4 tetrahedra (i.e. second-nearest neighbours of the central Si atom). Since Al and Si scatter x-rays almost identically the difference is not easily detected by XRD. In silicate materials the bonding of the SiO_4 groups can be denoted by their connectivity and given the designation Q^n. For example, in a chain silicate such as α-spodumene the local structural unit is denoted Q^2, referring to the two Si atoms in the chain on either side of the O atoms tetrahedrally bonded to the central Si. Similarly the local configuration in a three-dimensional structural silicate is denoted Q^4. For aluminosilicates, in which there is Al, Si interchange, additional distinctions need to be made to describe the second-nearest-neighbour coordination shell around the Si of the SiO_4 group. These are described as $Q^n(m\text{Al})$, where in a Q^n arrangement, m of the possible n second-nearest-neighbour Si have been replaced by Al. In a three-dimensional framework silicate there may be up to five, $Q^4(0\text{Al})$, $Q^4(1\text{Al})$, ..., $Q^4(4\text{Al})$, such configurations. The power of ^{29}Si NMR is that not only the main Q^n configurations, but also the $Q^n(m\text{Al})$ subconfigurations, are distinguishable by their chemical shift [5].

In the natural mineral α-spodumene, a chain silicate, there is complete Al, Si ordering with only one of the three $Q^2(m\text{Al})$ configurations present in the ^{29}Si spectrum, which is a single sharp line (see figure 4(a)); structural considerations indicate $m = 1$. In the glass phase the many configurations present lead to a broad ^{29}Si line (figure 4(b)). The spectrum recorded from the partially crystallized glass combines the broad line of the glass with the $Q^4(m\text{Al})$ configurations of the β-quartz SS (figure 4(c)). In the β-quartz SS phase there is only one distinguishable (Al, Si) site [2], and all five $Q^4(m\text{Al})$ configurations are present (figure 4(d)). A simulation of the peak areas was performed using the Bruker program LINESIM. The population of the various m values (the I_m distribution) is constrained by Loewenstein's rule for aluminosilicates from which one can derive equation (1) [15].

$$\frac{[\text{Si}]}{[\text{Al}]} = \sum_{m=1}^{4}[I_m] \Big/ \sum_{m=0}^{m=4}\left[\tfrac{1}{4}mI_m\right]. \tag{1}$$

The five-gaussian fit to the β-quartz SS powder lineshape gives values of the relative peak areas (I_m) of 4.5, 21.4, 38.6, 29.4 and 6.1 for the five peaks from left to right in figure 4(d). Knowing the Si:Al ratio (2:1) allows evaluation of the accuracy of Loewenstein's rule which for this case gives a value of 2.1:1 in good agreement. The I_m values of the β-quartz SS phase component lines change slightly as the annealing temperature is raised from 725 °C to 900 °C. In the β-spodumene SS phase there are two types of (Al, Si) site per unit cell, with twice as many of one site as the other [3]. The observed ^{29}Si spectrum for the β-spodumene SS phase is rather less well resolved than for the β-quartz SS phase and suggests that the five-line $Q^4(m\text{Al})$ spectrum for each of the two sites nearly overlap but with a small relative displacement (figure 4(e)). It is interesting to note the approximately 8 ppm displacement of the centre of gravity of the spectrum of the glass phase relative

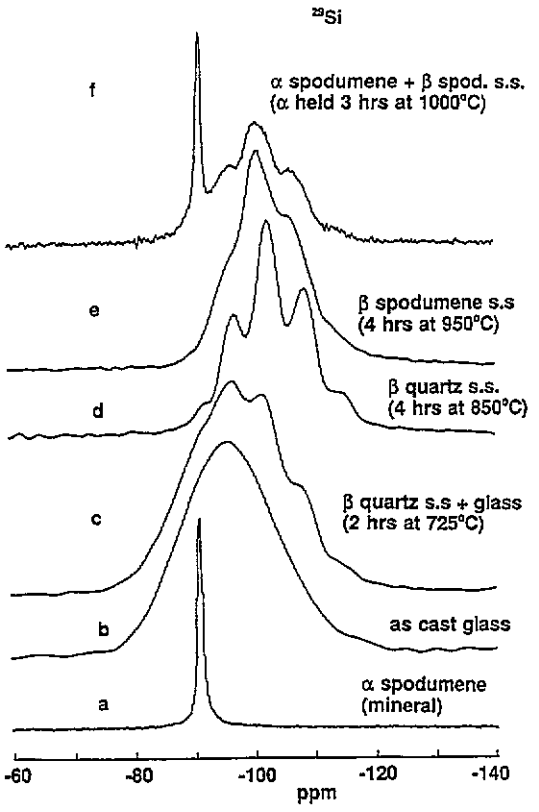

Figure 4. ^{29}Si NMR spectra recorded from (a) α-spodumene mineral, (b) as-cast glass, (c) β-quartz SS + glass, (d) β-quartz SS, (e) β-spodumene SS and (f) α-spodumene + β-spodumene SS.

to that of the β-quartz SS phase; a smaller shift is observed for β-spodumene SS phase. A similar displacement has been noted for other lithium aluminium silicate systems [16]. Evidently the predominant $Q^4(m\text{Al})$ configuration for the crystalline glass ceramic is not the same as for the glass. The ^{29}Si line from the Q^2 configuration in the chain silicate α-spodumene is shifted relative to the spectra of the Q^4 configurations of the framework silicas as might be expected. An order–disorder transformation occurs on annealing pure α-spodumene mineral for 3 h at 1000 °C well below the melt temperature of 1600 °C. The spectrum changes from one sharp resonance indicative of unique atomic positions to the β-spodumene SS structure in which random Si, Al atomic interchange occurs. This spectral change is similar to that observed for the glass ceramic annealed above 900 °C (see figure 4(a), (e), (f)).

The ^{27}Al NMR spectra shown in figure 5 (a)–(d) are less informative about the details of the order–disorder processes occurring in the glass, β-quartz SS and β-spodumene SS phases but do give a clear indication of the O coordination of the Al. The Al in α-spodumene is octahedrally co-ordinated by O as indicated by the shift and shown by the x-ray structure [17]. The structure in the spectrum (figure 5(a)) is due to a well defined nuclear quadrupole interaction at all Al sites, i.e. from an atomically ordered crystal. The nuclear quadrupole coupling constant for the ^{27}Al, derived from simulating the powder lineshape, is approximately e^2qQ/h ($\equiv C_q$) = 3.1 MHz with asymmetry parameter $\eta = 0.97$, agreeing reasonably well with the published single-crystal values [18]. The chemical shift parameter is $\delta = 3.0$ ppm, which does not seem to have been published. The line shape simulation indicates the presence of a small amount of an Al-containing impurity phase in the α-

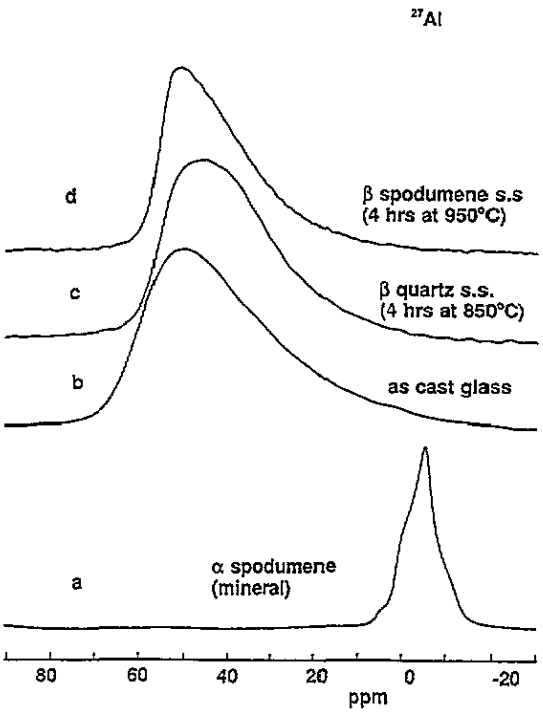

Figure 5. ^{27}Al NMR spectra recorded from (a) α-spodumene mineral, (b) as-cast glass, (c) β-quartz SS and (d) β-spodumene SS.

spodumene.

In the glass, β-quartz SS and β-spodumene SS phases derived from the melt or by annealing α-spodumene, the Al is tetrahedrally coordinated by O. The ^{27}Al lineshape for these phases is asymmetric and characteristic of a disordered system where there is a distribution of (C_q, η) [19, 20], with a peak at approximately 51 ppm (figure 5(b)–(d)). The distribution of (C_q, η) is caused principally by the random interchange of Al and Si in the second co-ordination shell around the central Al. The line shape for the glass is very similar in shape and half-width to that for the β-quartz SS and β-spodumene SS phases, which have ordered lattices, thereby indicating that (C_q, η) is the main line shape determinant.

3.3. PALS

Twelve samples were studied by PALS; they are listed in table 2 with the results from the fitting program. The results are mean values for the number of spectra which could be reasonably fitted with three free components; population standard deviations are given in brackets. Six of the samples had four or fewer spectra reasonably fitted by the free three-component fit. For these six samples, marked with an asterisk in table 2, the fitting routine was rerun with the short lifetime τ_1 fixed at the mean value of τ_1 calculated from the spectra that did converge during the free fit.

As stated in the introduction, the lifetime spectra of inorganic glasses can typically be modelled as the sum of two or three decaying exponentials. For the case of a three-component fit, the mean lifetime, τ_m, is calculated using equation (2):

$$\tau_m = \frac{I_1\tau_1 + I_2\tau_2 + I_3\tau_3}{I_1 + I_2 + I_3}. \tag{2}$$

Table 2. Three free-lifetime fits for LAS glass ceramics and α-spodumene mineral (population standard deviation in brackets). Note: an asterisk (*) denotes that the fitting routine was rerun with the short lifetime τ_1 fixed at the mean value of τ_1 calculated from the spectra that did converge during the free fit.

Sample	No. of converged runs/total runs	Bulk lifetime component		Trapped lifetime component		oPs lifetime component		Mean lifetime
		τ_1 (ps)	I_1 (%)	τ_2 (ps)	I_2 (%)	τ_3 (ns)	I_3 (%)	τ_m (ps)
as-cast glass	7/8	215 (13)	21.7 (2)	435 (3)	77.6 (2)	2.11(.4)	0.68 (.14)	400 (2)
1 hr 725°C	3/4	223 (9)	34.6 (4)	440 (7)	63.4 (4)	2.65 (.1)	2.0 (.06)	411 (2)
	*4/4	*223 fixed	*35.6 (1)	*440 (2)	*63.4 (1)	*2.67(.1)	*2.0(.05)	*411 (2)
1.5 hr 725°C	6/6	191 (7)	36.0 (2)	427 (6)	61.0 (2)	2.43 (.1)	3.0 (.1)	401 (2)
4 hr 725°C	6/7	202 (32)	18.8 (6)	438 (18)	75.7(4.4)	1.06 (.1)	5.5 (1.5)	427 (2)
6 hr 725°C	3/4	208 (7)	53.1 (4)	372 (7)	45.2 (4)	2.82(.01)	1.7 (.02)	326 (2)
	*4/4	*208 fixed	*51.9 (2)	*369 (6)	*46.4(2)	*2.8(.05)	*1.7(.04)	*327 (2)
8 hr 725°C	1/5	206	18.3	337	81.3	1.48	0.48	319
	*4/5	*206 fixed	*20.7(4)	*341 (7)	*79 (4)	*2.3 (1)	*0.4 (.1)	*319 (2)
16 hr 725°C	4/10	201 (28)	22.4(10)	337 (11)	77.1(10)	1.9(.05)	0.47(.03)	316(1)
	*9/10	*201 fixed	*18.0 (3)	*332 (4)	*81.5 (3)	*1.8 (.3)	*0.52(.1)	*316(2)
4 hr 750°C	10/10	207 (23)	35.0 (10)	349 (13)	63.8 (10)	2.3 (.2)	1.2 (.1)	323 (2)
4 hr 850°C	5/10	205 (14)	41.6 (5)	350 (6)	56.7 (5)	2.5 (.16)	1.7 (.1)	326 (2)
4 hr 950°C	8/10	204 (20)	30.3 (9)	341 (10)	68.9 (9)	2.4 (.3)	0.8 (.07)	318 (2)
spodumene mineral	3/9	218 (4)	82.0 (6)	331 (15)	17.7 (6)	2.6 (.3)	0.2 (.03)	240 (2)
	*7/9	*218 fixed	*82 (2)	*320 (10)	*18 (3)	*2.3 (.5)	*0.2 (.1)	*240 (2)
3 hr 1000°C mineral	3/6	208 (10)	39.6 (3)	365 (1)	59.8 (3)	1.6 (.3)	0.6 (.1)	310 (2)
	*5/6	*208 fixed	*36.9 (4)	*356(10)	*62.0 (4)	*1.2 (.3)	*1.1 (.4)	*310 (2)

The mean lifetime, τ_m, (with intensity of 100%) is displayed in table 2. Identification of the positron annihilation sites contributing to the mean lifetime is possible by comparison of the lifetime values with those found in other glass and ceramic systems. The short lifetimes, τ_1, in table 2 can be attributed to free positrons annihilating in the bulk glass or ceramic with a small contribution from pPs self-annihilation. It is interesting to note that the electron densities at the annihilation sites of free positrons ($\tau_1 = 207 \pm 8$ ps) are similar for the glass, partially crystallized glasses and spodumene mineral. Previous PALS work by Hautojarvi and Pajanne [9] on LAS glass reported two lifetime components for a Li_2O–Al_2O_3–SiO_2 material with composition ratio 2:1:7. The two-component fit gave τ_1 values ranging from 280 ps to 306 ps and τ_2 values varying from 680 ps to 890 ps as functions of heat treatment at 600 °C which caused crystallization. The short-lifetime component (τ_1, I_1) was attributed to the annihilation of free positrons. The trapped positron component (τ_2, I_2) was tentatively attributed to a positron–negative oxygen ion bound state in the glass phase, and the intensity of this component, I_2, decreased with increasing crystallinity. The composition of the LAS glass in the work of Hautojarvi and Pajanne [9] is so different from that of the present work that the differences in PALS results are not surprising. A study of lithium disilicate glass and glass ceramics by James *et al* [21] reported three lifetime components ($\tau_1 = 280$–300 ps, $\tau_2 = 590$–630 ps, $\tau_3 = 1.7$–2.3 ns). The study showed that I_2 was a linear function of molar free volume (estimated from density) [21]. A positron study of glass ceramics made by the devitrification of cordierite glass ($13.3MgO{\cdot}32Al_2O_3{\cdot}52.7SiO_2 \cdot 2BaO$) [22] reported two lifetime components: $\tau_1 = 330$–370 ps, $\tau_2 = 530$–880 ps. The study of cordierite was performed as a function of temperature, and both components were sensitive to crystallization (at the crystallization temperature). The short-lifetime component was attributed to free positrons and pPs, and the longer-lifetime component was attributed to oPs pickoff annihilation in free volume sites. The assignment of τ_2 to oPs pickoff in [22] and to a positron–anion bound state in [9] gives an indication of the disagreement as to the origin of the approximately 300–900 ps component in ionic solids [23]. It is postulated that the second lifetime component in the present work is due to positron–oxygen bound states or to positrons trapped at vacancy-type defects or interatomic sites. The second lifetime component (τ_2, I_2) in the as-cast glass and the partially crystallized samples is $\tau_2 = 0.430 \pm 0.01$ ns, whilst in the fully crystalline samples $\tau_2 = 0.350 \pm 0.02$ ns. The decrease in τ_2 which is shown in figure 6 is indicative of the increase in local electron density at the annihilation site due to improved packing (on crystallization). Most likely, more than one annihilation mechanism contributes to the intermediate-lifetime component ($\tau_2 = 330$–440 ps) in the present work, but a discussion of the PALS results in relation to the packing of the glass ceramic seems reasonable as illustrated by the following comparison of mean lifetime and density. However, it should be noted that PALS studies of cordierites [22, 24] have attributed changes in the 300–500 ps component to Al, Si order processes.

The variation in the crystalline structure as a function of annealing temperature, β-quartz SS or β-spodumene SS, has a minimal effect on molar volume and, hence, is not expected to affect the PALS results. As mentioned in the introduction, the densities of these two crystalline phases are similar; however, they are 33% less dense than the α-spodumene crystalline phase. It is interesting to note that this variation in packing is similar to the variation in mean lifetime values in table 2 which shows a 33% increase in mean lifetime commensurate with the change in density: $\tau_m = 240$ ps for α-spodumene, $\tau_m = 318$ ps for β-spodumene SS and $\tau_m = 316$–326 ps for β-quartz SS

The partially crystallized glasses contain an appreciable oPs pickoff component ($I_3 > 1\%$). In previous work on glasses and glass ceramics [22, 25] the oPs pickoff component intensity has varied with molar volume during crystallization of glasses leading to the

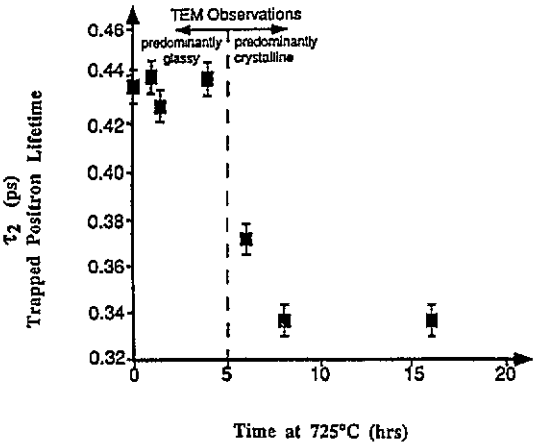

Figure 6. The second lifetime, τ_2, as a function of heat treatment time at 725 °C.

postulate that this component is associated with the free volume of the system. According to the free volume model [26] the value of τ_3 gives an indication of the mean size of the free volume sites and that of I_3 reflects the relative concentration of free volume [25,27]. Unlike the glasses in these previous studies, the as-cast glass in this work has a negligible oPs pickoff component ($I_3 < 1\%$). As shown in figure 7, the PALS results indicate that the oPs pickoff component intensity, I_3, is sensitive to the nucleation and hence formation of the glass ceramic. The as-cast glass and the fully crystalline samples exhibit negligible oPs intensity, I_3, whilst the partially crystallized samples show an increasing oPs intensity with time at 725 °C up to 4 h. Hence correlation with the TEM observations in figure 3 indicates that the oPs component is associated either with the nuclei/glass interface or with the nuclei composition and structure. The potential of PALS to examine microstructural changes during the processing of glass ceramics has been illustrated and will be investigated further in future work.

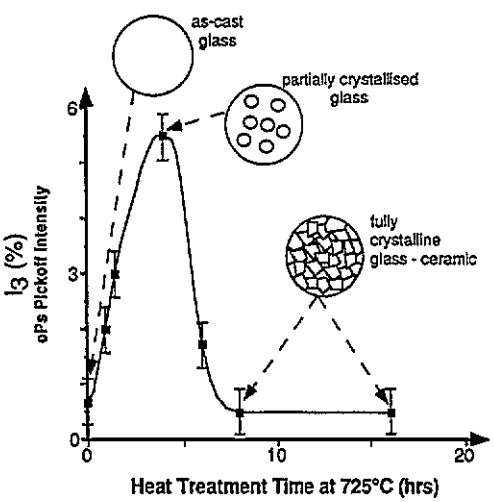

Figure 7. The intensity of the oPs pickoff component, I_3, as a function of heat treatment time at 725 °C.

In nanocrystalline metal alloys, the intermediate PALS component (τ_2 = 200–400 ps) has been used to follow interfacial free volume [28–31]. In Fe alloys [29], the PALS measurement of nanovoids at the grain boundaries has been used to indicate the maximum volume and minimum density for a particular grain size. The variation in nanovoid density

at the interface (as measured by PALS) has been correlated with microhardness indicating that not only grain size but also interface structure are important to mechanical properties of nanocrystalline materials [28–31]. Nanohardness measurements of the LAS glass and glass ceramics have been performed and have been published elsewhere [33]. Future PALS studies of these glass ceramics will attempt to establish a causal relationship between the PALS indications of packing-related structure and the mechanical properties, similar to the approach taken by Schaefer and co-workers [30–32] in PALS studies of nanocrystalline metals.

4. Conclusion

Use of NMR, PALS, TEM and XRD to characterise the structure of glasses and glass ceramics has highlighted the individual and combined strengths of these techniques. The characterization of the effect of processing on structure and properties of LAS glass ceramics prepared from natural spodumene mineral can aid fabrication technology for the production of glass ceramics from this abundant raw material.

Acknowledgments

The authors wish to thank Dr M E Smith for helpful discussions. The PALS work was funded by the Australian Research Council. AN is grateful to the Australian government and Monash University for financial support.

References

[1] Scheidler H and Rodek E 1989 *Am. Ceram. Soc. Bull.* **68** 1926
[2] Li Chi-Tang and Peacor D R 1968 *Z. Kristallogr.* **126** 46
[3] Li Chi-Tang 1968 *Z. Kristallogr.* **127** 327
[4] Cameron M, Sueno S, Prewitt C T and Papike J J 1973 *Am. Mineral.* **58** 594
[5] Engelhardt G and Michel D 1987 *High Resolution Solid State NMR of Silicates and Zeolites* ed G Engelhardt (New York: Wiley) ch 4
[6] Slichter C P 1990 *Principles of Magnetic Resonance* (New York: Springer) ch 8, 9
[7] Siegel R W 1980 *Annu. Rev. Mater. Sci.* **10** 393
[8] Goldanskii V I 1968 *At. Energy Rev.* **6** 3
[9] Hautojarvi P and Pajanne E 1974 *J. Phys. C: Solid State Phys.* **7** 3817
[10] Hill A J, Newman P J, Javorniczky J and MacFarlane D R 1994 *J. Non-Cryst. Solids* **177** 277
[11] Forster M, Claudy W, Hermes H, Koch M, Maier K, Major J, Stoll H and Schaefer H-E 1992 *Mater Sci. Forum* **105–110** 1005
[12] Hautojarvi P, Vehanen A, Komppa V and Pajanne E 1978 *J. Non-Cryst. Solids* **29** 365
[13] Puff W 1983 *Comput. Phys. Commun.* **30** 359
[14] Eldrup M 1971 *RISO Report* 254, p 37
[15] Magi M, Lipmaa E, Samoson A, Engelhardt G and Grimmer A-R 1984 *J. Phys. Chem.* **88** 1518
[16] Parot-Rajaona T, Coté B, Bessada C, Massiot D and Gervais F 1994 *J. Non-Cryst. Solids* **169** 1
[17] Wyckoff R W G (ed) 1968 *Crystal Structures* 2nd edn, vol 4 (New York: Interscience) p 170
[18] Smith M E 1993 *Appl. Magn. Reson.* **4** 1
[19] Jaeger C, Kunath G, Losso P and Scheler G 1993 *Solid State NMR* **2** 73
[20] Kohn S C, Dupree R and Smith M E 1989 *Geochim. Cosmoschim. Acta* **53** 2925
[21] James P F, Paul A, Singru R M, Dauwes C, Dorikens-Vanpraet L and Dorikens M 1975 *J. Phys. C: Solid State Phys.* **8** 393
[22] Pedrosa M A and Pareja R 1985 *J. Mater. Sci.* **20** 4501
[23] Jensen K O, Salmon P S, Penfold I T and Coleman P G 1994 *J. Non-Cryst. Solids* **170** 57
[24] Hsu F S and Vance E R 1980 *Phys. Chem. Miner.* **6** 47
[25] Singh K P, Singru R M and Rao C N R 1972 *J. Phys. C: Solid State Phys.* **5** 1067

[26] Brandt W 1967 *Positron Annihilation* ed A T Stewart and L O Roellig (New York: Academic) p 155
[27] Singh K P, West R N and Paul A 1976 *J. Phys. C: Solid State Phys.* **9** 305
[28] Sui M L and Lu K 1993 *ICAM'93 (Tokyo, 1993)* paper BB2-7
[29] Liu X D, Wang J T, Hu Z Q and Ding B Z 1993 *Mater. Sci. Eng.* A **169** L17
[30] Schaefer H-E and Wurschum R 1987 *Phys. Lett.* **119A** 370
[31] Schaefer H-E, Wurschum R, Birringer R and Gleiter H 1988 *Phys. Rev.* B **38** 9545
[32] Wurschum R, Greiner W and Schaefer H-E 1993 *Nanostruct. Mater.* **2** 55
[33] Nordmann A 1994 *Department of Materials Engineering, Monash University Internal Report*